



Article

Building and Breaking Bonds by Homogenous Nucleation in Glass-Forming Melts Leading to Transitions in Three Liquid States

Robert F. Tournier ^{1,*}  and Michael I. Ojovan ^{2,3} ¹ LNCMI-EMFL, CNRS, Université Grenoble Alpes, INSA-T, UPS, 38042 Grenoble, France² Department of Materials, Imperial College London, London SW7 2AZ, UK; m.ojovan@imperial.ac.uk³ Department of Radiochemistry, Lomonosov Moscow State University, 119991 Moscow, Russia

* Correspondence: robert.tournier@lncmi.cnrs.fr

Abstract: The thermal history of melts leads to three liquid states above the melting temperatures T_m containing clusters—bound colloids with two opposite values of enthalpy $+\Delta\varepsilon_{lg} \times \Delta H_m$ and $-\Delta\varepsilon_{lg} \times \Delta H_m$ and zero. All colloid bonds disconnect at $T_{n+} > T_m$ and give rise in congruent materials, through a first-order transition at $T_{LL} = T_{n+}$, forming a homogeneous liquid, containing tiny superatoms, built by short-range order. In non-congruent materials, (T_{n+}) and (T_{LL}) are separated, T_{n+} being the temperature of a second order and T_{LL} the temperature of a first-order phase transition. (T_{n+}) and (T_{LL}) are predicted from the knowledge of solidus and liquidus temperatures using non-classical homogenous nucleation. The first-order transition at T_{LL} gives rise by cooling to a new liquid state containing colloids. Each colloid is a superatom, melted by homogeneous disintegration of nuclei instead of surface melting, and with a Gibbs free energy equal to that of a liquid droplet containing the same magic atom number. Internal and external bond number of colloids increases at T_{n+} or from T_{n+} to T_g . These liquid enthalpies reveal the natural presence of colloid–colloid bonding and antibonding in glass-forming melts. The Mpemba effect and its inverse exist in all melts and is due to the presence of these three liquid states.

Keywords: liquid–liquid transitions; glass phase; amorphous; undercooling; superheating; percolation threshold; microheterogeneity



Citation: Tournier, R.F.; Ojovan, M.I. Building and Breaking Bonds by Homogenous Nucleation in Glass-Forming Melts Leading to Transitions in Three Liquid States. *Materials* **2021**, *14*, 2287. <https://doi.org/10.3390/ma14092287>

Academic Editor: Gerhard Wilde

Received: 26 March 2021

Accepted: 26 April 2021

Published: 28 April 2021

Publisher's Note: MDPI stays neutral with regard to jurisdictional claims in published maps and institutional affiliations.



Copyright: © 2021 by the authors. Licensee MDPI, Basel, Switzerland. This article is an open access article distributed under the terms and conditions of the Creative Commons Attribution (CC BY) license (<https://creativecommons.org/licenses/by/4.0/>).

1. Introduction

Glass-forming melt transformations have been mainly studied, for many years, around the glass transition temperature T_g and sometimes up to the liquidus temperature T_{liq} . The liquid properties are often neglected because the classical nucleation equation predicts the absence of growth nuclei and nucleation phenomenon above the melting temperature. The presence of growth nuclei above T_m being known [1–3], an additional enthalpy is added to this equation to explain these observations. A new model of nucleation is built from the works of Turnbull's [4] characterized by two types of homogeneous nucleation temperatures below and above T_m . The new additional enthalpy is a quadratic function of the reduced temperature $\theta = (T - T_m)/T_m$ as shown by a revised study of the maximum undercooling rate of 38 liquid elements using Vinet's works [5,6]. A concept of two liquids is later introduced to explain the glass phase formation at T_g by an enthalpy decrease from liquid 1 to liquid 2 at this temperature. New laws minimizing the numerical coefficients of each quadratic equation are established determining the enthalpies $\varepsilon_{ls}(0) \times \Delta H_m$ of liquid 1 and $\varepsilon_{gs}(0) \times \Delta H_m$ of liquid 2 for each θ value, with ΔH_m being the melting enthalpy [7,8]. The thermodynamic transition at T_g is characterized by a second-order phase transition and a heat capacity jump defined by the derivative of the difference $(\varepsilon_{ls}(\theta) - \varepsilon_{gs}(\theta)) \Delta H_m$ which is equal to $1.5 \Delta S_m$ for many glass transitions with ΔS_m being the melting entropy [9].

The glass transition results from the percolation of superclusters formed during cooling below T_m [10–12]. A thermodynamic transition characterized by critical parameters occurs by breaking bonds (configurons) and when the percolation threshold of configurons

is attained [13–17]. Building bonds by enthalpy relaxation below T_g has for consequence the formation of a hidden undercooled phase called phase 3 with an enthalpy $(\epsilon_{ls}(\theta) - \epsilon_{gs}(\theta)) \Delta H_m$ equal to that of configurons with a residual bond fraction which can be overheated up to $T_{n+} > T_m$ before being melted [18]. The homogeneous nucleation temperature at T_{n+} occurs in overheated liquids and is predicted for many molecular and metallic glass-forming melts.

This paper is devoted to phase transitions above T_m completing our recent work, showing that the dewetting temperatures of prefrozen and grafted layers in ultrathin films are equal to T_{n+} [19]. The latent heats are exothermic or endothermic without knowing the explanation. The existence of a first-order transition is claimed for $Pd_{42.5}Ni_{42.5}P_{15}$ and $La_{50}Al_{35}Ni_{15}$ liquid alloys [20,21]. Our nucleation model of melting the liquid mean-range order by breaking residual bonds predicted all values of T_{n+} and exothermic enthalpies at this temperature. The observation of endothermic latent heats showed the existence of three liquid states at T_m , the first one with a positive enthalpy $\epsilon_{gs}(0) \times \Delta H_m$, the second one zero, and the third one $-\epsilon_{gs}(0) \times \Delta H_m$, which is negative. The liquid is homogeneous above T_{n+} when its enthalpy is equal to zero. The existence of various liquid states was also predicted without using a non-classical nucleation equation [22]. The formation temperature of a homogeneous liquid state was observed by measuring the density or the viscosity during heating and cooling, determining the point where the branching of these quantities disappears. Colloidal states were observed below this homogenization temperature and composed of thousands of atoms defining liquid heterogeneities [23–27]. Our objectives were to predict all these phase transitions.

2. The Homogeneous Nucleation

The Gibbs free energy change for a nucleus formation in a melt was given by Equation (1) [6,9]:

$$\Delta G_{ls} = (\theta - \epsilon_{ls}) \Delta H_m / V_m \times 4\pi R^3 / 3 + 4\pi R^2 \sigma_{ls} \quad (1)$$

where R is the nucleus radius and following Turnbull [4], σ_{ls} its surface energy, given by Equation (2), θ the reduced temperature $(T - T_m) / T_m$, ΔH_m the melting enthalpy at T_m , and V_m the molar volume:

$$\sigma_{ls} (V_m / N_A)^{-1/3} = \alpha_{ls} \Delta H_m / V_m \quad (2)$$

A complementary enthalpy $-\epsilon_{ls} \times \Delta H_m / V_m$ was introduced, authorizing the presence of growth nuclei above T_m . The classical nucleation equation was obtained for $\epsilon_{ls} = 0$.

The critical radius R_{ls}^* in Equation (3) and the critical thermally activated energy barrier $\frac{\Delta G_{ls}^*}{k_B T}$ in Equation (4) are calculated assuming $d\epsilon_{ls} / dR = 0$:

$$R_{ls}^* = \frac{-2\alpha_{ls}}{(\theta - \epsilon_{ls})} \left(\frac{V_m}{N_A} \right)^{-1/3} \quad (3)$$

$$\frac{\Delta G_{ls}^*}{k_B T} = \frac{16\pi \Delta S_m \alpha_{ls}^3}{3N_A k_B (1 + \theta)(\theta - \epsilon_{ls})^2} \quad (4)$$

These critical parameters are not infinite at the melting temperature T_m because ϵ_{ls} is not equal to zero. The nucleation rate $J = K_v \exp(-\frac{\Delta G_{ls}^*}{k_B T})$ is equal to 1 when Equation (5) is respected:

$$\Delta G_{ls}^* / k_B T = \ln(K_v) \quad (5)$$

The surface energy coefficient α_{ls} in Equation (2) is determined from Equations (4) and (5) and given by Equation (6):

$$\alpha_{ls}^3 = \frac{3N_A k_B (1 + \theta)(\theta - \epsilon_{ls})^2}{16\pi \Delta S_m} \ln(K_v) \quad (6)$$

The nucleation temperatures θ_n obtained for $d\alpha_{1s}^3/d\theta = 0$ obeys (7):

$$d\alpha_{1s}^3/d\theta \sim (\theta_{n+} - \varepsilon_{1s})(3\theta_{n-} + 2 - \varepsilon_{1s}) = 0 \quad (7)$$

In addition to the nucleation temperature T_{n-} below T_m , the existence of homogeneous nucleation up to T_{n+} above T_m was confirmed by many experiments, observing the undercooling versus the overheating rates of liquid elements and CoB alloys [28,29]. This nucleation temperature could have, for consequence, the possible existence of a second melting temperature of growth nuclei above T_m and of their homogeneous nucleation at temperatures weaker than θ_{n+} .

The coefficient ε_{1s} of the initial liquid called liquid 1 is a quadratic function of θ in Equation (8) [6]:

$$\varepsilon_{1s} = \varepsilon_{1s0}(1 - \theta^2/\theta_{0m}^2) \quad (8)$$

where θ_{0m} is the Vogel–Fulcher–Tammann-reduced temperature leading to $\varepsilon_{1s} = 0$ for $\theta = \theta_{0m}$, the VFT temperature T_{0m} of many fragile liquids being equal to $\cong 0.77 T_g$. This quasi-universal value is known for numerous liquids including atactic polymers [30,31].

New liquid states are obtained for $\theta = \theta_{n+} = \varepsilon_{1s}$ and $\theta = \theta_{n-} = (\varepsilon_{1s} - 2)/3$ with Equation (7). The reduced nucleation temperatures θ_{n-} are solutions of the quadratic Equation (9):

$$\varepsilon_{1s0}\theta_{n-}^2/\theta_{0m}^2 + 3\theta_{n-} + 2 - \varepsilon_{1s0} = 0 \quad (9)$$

There is a minimum value of ε_{1s0} plotted as function of θ_{0m} using (8) and $\theta_{n-} = (\varepsilon_{1s} - 2)/3$, determining the relation (10) between θ_{0m}^2 and ε_{1s0} for which the two solutions of (9) are equal in the two fragile liquids [8,32]. These values defined the temperature where the surface energy was minimum and θ_{0m}^2 and ε_{1s0} obeyed Equations (10) and (11):

$$\theta_{0m}^2 = \frac{8}{9}\varepsilon_{1s0} - \frac{4}{9}\varepsilon_{1s0}^2 \quad (10)$$

$$\varepsilon_{1s}(\theta = 0) = \varepsilon_{1s0} = 1.5\theta_{n-} + 2 = a\theta_g + 2 \quad (11)$$

The value $a = 1$ in the Equation (10) leads to $T_{0m} = 0.769 \times T_g$ in agreement with many experimental values [9].

All melts and even liquid elements underwent, in addition, a glass transition because another liquid 2 existed characterized by an enthalpy coefficient ε_{gs} given by Equation (12), inducing an enthalpy change from that of liquid 1 at the thermodynamic transition at T_g [7,9,32]:

$$\varepsilon_{gs} = \varepsilon_{gs0}(1 - \theta^2/\theta_{0g}^2) \quad (12)$$

$$\theta_{0g}^2 = \frac{8}{9}\varepsilon_{gs0} - \frac{4}{9}\varepsilon_{gs0}^2 \quad (13)$$

$$\varepsilon_{gs}(\theta = 0) = \varepsilon_{gs0} = 1.5\theta_{n-} + 2 = 1.5\theta_g + 2 \quad (14)$$

The difference $\Delta\varepsilon_{lg}$ in the Equation (15) between the coefficients ε_{1s} and ε_{gs} determines the phase 3 enthalpy when the quenched liquid escapes crystallization:

$$\Delta\varepsilon_{lg}(\theta) = \varepsilon_{1s} - \varepsilon_{gs} = \varepsilon_{1s0} - \varepsilon_{gs0} + \Delta\varepsilon - \theta^2 \left(\frac{\varepsilon_{1s0}}{\theta_{0m}^2} - \frac{\varepsilon_{gs0}}{\theta_{0g}^2} \right) \quad (15)$$

The coefficient $\Delta\varepsilon_{lg}(\theta)$ defined a new liquid phase called phase 3 undergoing a hidden phase transition below T_g and a visible one at θ_{n+} , occurring for $\Delta\varepsilon_{lg}(\theta) = \theta_{n+}$, as shown by Equation (7). This transition was accompanied by an exothermic latent heat equal to $\Delta\varepsilon_{lg}(\theta) \times \Delta H_m$ corresponding to about 15% of the melting heat [18]. Phase 3 was detected for the first time in supercooled water and associated with glacial phase formation [33–35] and recently appears as being associated with configuron formation [13–18]. The concept of configurons was initially proposed for materials with covalent bonds which can be either

intact or broken [36]; then, it was extended to other systems including metallic systems based on ideas of Egami on bonds between nearest atoms in metals [16,37]. Thus, it is generically assumed that the set of bonds in condensed matter has two states; namely, the ground state corresponding to unbroken bonds and the excited state corresponding to broken bonds. The set of bonds in condensed matter is described in such a way by the statistics of a two-level system [38,39] which are separated by the energy interval G_d . The two approaches converge because the Gibbs free energy of phase 3 is equal to G_d . Phase 3 is assumed to be the configuron phase which is preserved above T_m in a liquid with medium-range order up to a temperature T_{n+} . Both transition temperatures T_g and T_{n+} are accompanied by enthalpy or entropy changes of phase 3 and are predicted in many cases: Annealing above and below T_g , vapor deposition, formation of glacial and quasi-crystalline phases in perfect agreement with experiments. Any transformation of phase 3 changes the initial liquid enthalpy and rejuvenation at $T_g < T < T_{n+}$ does not lead to the enthalpy of the initial liquid [18].

Our new publication here was devoted to the simplest case where ultrastable glass and glacial phase are not formed. The value of θ_{n+} was maximum in this case because all transformations below T_g and T_m modified the liquid state and decrease θ_{n+} [19].

The heat capacity jump at T_g was equal to $1.5 \times \Delta H_m/T_m$ in polymers as shown in 1960 by Wunderlich [40] and confirmed for many molecular glasses [9] (where $\Delta H_m/T_m = \Delta S_m$ is the crystal melting entropy). The contribution of the undercooled liquid to the total heat capacity per mole is given by (16) using $d\Delta\epsilon_{lg}(\theta)/dT$:

$$\Delta C_p(T) = C_p(\text{liq}) - C_p(\text{cryst}) = 2 \frac{(T - T_m)}{T_m^2} (\Delta H_m) \left(\frac{\epsilon_{ls0}}{\theta_{0m}^2} - \frac{\epsilon_{gs0}}{\theta_{0g}^2} \right) \quad (16)$$

3. Exothermic or Endothermic Heats Observed above the Melting Temperature T_m

3.1. Exothermic Enthalpy Delivered at 688 K in $Al_{88}Ni_{10}Y_2$ for $T_m = 602$ K

We follow data of ref. [41]. The glass transition occurs at $T_g = 380$ K, and the melting temperature at $T_m = 602$ K. In Figure 1, an annealing of 60 s at $T_a = 401, 427,$ and 525 K increases the fraction V_f of Al-fcc precipitates up to 0.42 and decreases the volume of the amorphous phase without changing the enthalpy recovery at 688 K measured at 0.67 K/s.

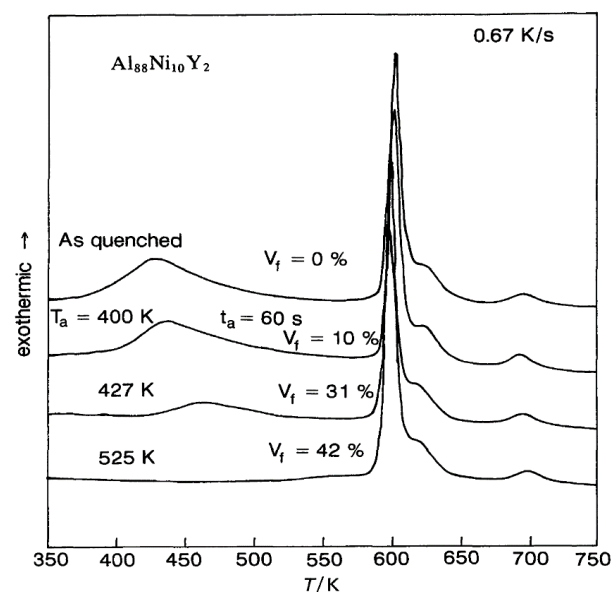


Figure 1. DSC curves measured at 0.67 K/s of an $Al_{88}Ni_{10}Y_2$ amorphous alloy aged for 60 s at different T_a . Reprinted from ref. [42], Figure 4.

3.2. Exothermic Enthalpy Delivered at $T_{n+} = 1622$ K in $(Fe_{71.2}B_{24}Y_{4.8})_{96}Nb_4$

We follow data of ref. [42]. The glass transition occurs at $T_g = 963$ K and the melting temperature at $T_m = 1410$ K. An enthalpy recovery occurs at 1622 K (Figure 2).

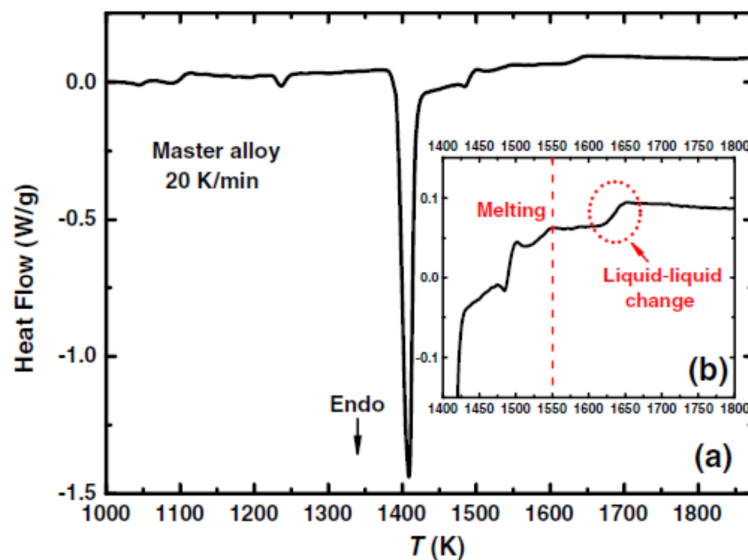


Figure 2. (a) High-temperature DSC trace at 0.33 K/s of the master alloy and (b) the enlarged version after melting. Reprinted with permission from ref. [42], Figure 7. Copyright 2014 Springer.

3.3. Exothermic Enthalpy Delivered at 1835 K in $Ni_{77.5}B_{22.5}$

We follow data of ref. [24]. The glass transition occurs at $T_g = 690$ K and the melting temperature at $T_m = 1361$ K. The enthalpy recovery temperature is equal to 1835 K.

Deep transformations of eutectic liquid state are observed in Figure 3 by slow heating and aging above the melting temperature which are attributed to the formation of microdomains of 10–100 nm enriched with one of the components with prolonged relaxation time. These microdomains have an influence on the structure and properties of rapidly quenched liquid alloys [24,25]. The enthalpy recovery temperature is here the highest temperature of liquid transformation leading to its homogeneous state. A cooling from 1950 K gives rise to a homogeneous liquid leading to supercooling below $T_m = 1361$ K.

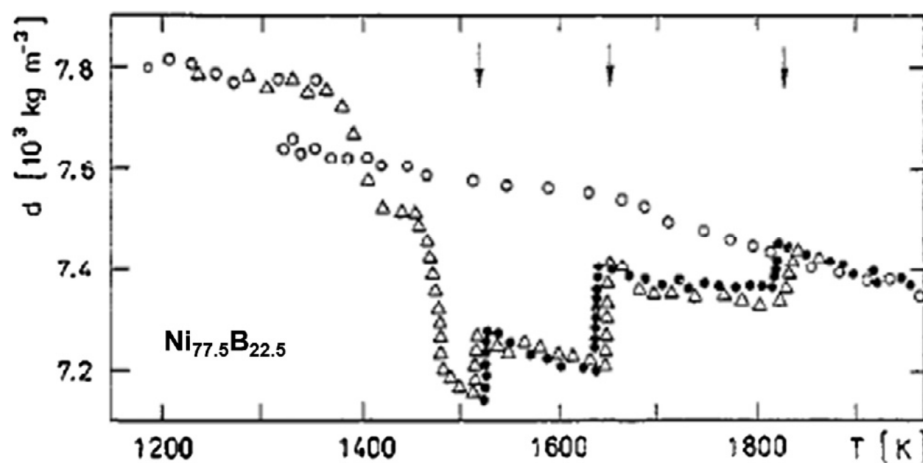


Figure 3. Temperature dependence of the density d of Ni-22.5%B melt at slow heating after melting and time exposition for 5–20 h (\bullet), subsequent cooling (\circ), and the second heating after crystallization of the sample and repeated melting (Δ). The arrows show the “critical” temperatures at which the density instability is observed. Reprinted with permission from ref. [24], Copyright 1997 Elsevier.

3.4. Exothermic Enthalpy Delivered at 1356 K in $\text{Cu}_{47.5}\text{Zr}_{45.1}\text{Al}_{7.4}$

We follow data of ref. [43]. The glass transition occurs at $T_g = 690$ K and the melting temperature at $T_m = 1170$ K. An enthalpy recovery occurs at 1356 K (Figure 4).

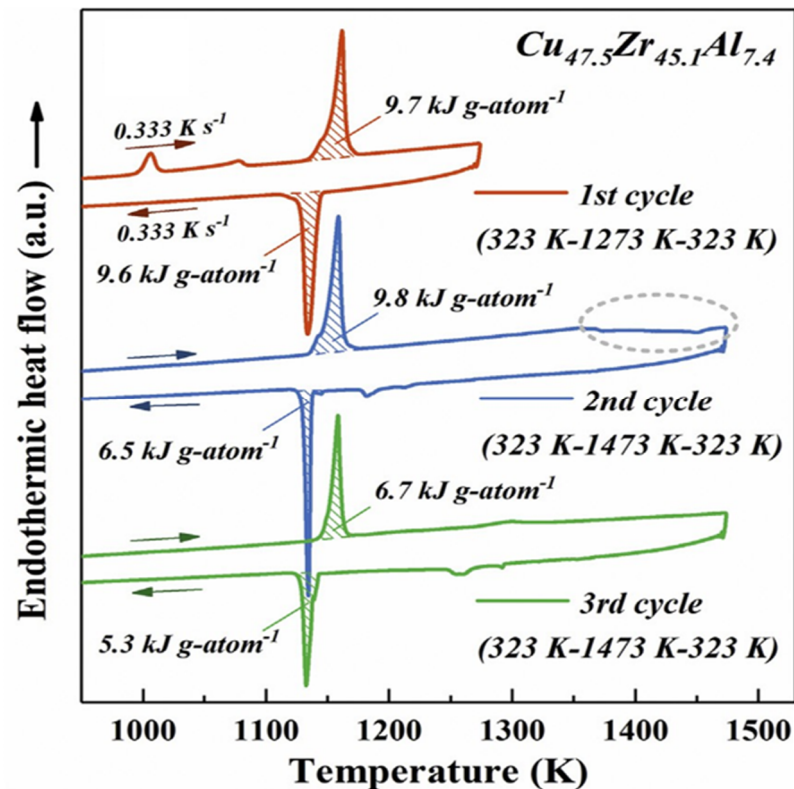


Figure 4. Multiple DTA measurements (0.333 K/s) of $\text{Cu}_{47.5}$ alloy. The first up- and down-scan cycle is well below 1350 K and the last two cycles reach 1473 K. A remarkable exothermic reaction observed at the temperature above 1350 K in the second up-scan curve is marked by a gray dashed circle. Reprinted with permission from ref. [43], Figure 9b, Copyright 2020 Elsevier.

3.5. Endothermic Enthalpy Recovered at 1453–1475 K in a Silicate Liquid

We follow data of ref. [44]. The composition was (49.3 SiO_2 , 15.6 Al_2O_3 , 1.8 TiO_2 , 11.7 FeO , 10.4 CaO , 6.6 MgO , 3.9 Na_2O , and 0.7 K_2O (wt%)). The glass transition occurred at $T_g = 908$ K and the melting temperature at $T_m = 1313$ K. The exothermic latent heat occurred at 1173 K and the amorphous fraction decline with the cycle number from 573 to 1523 K. The melting extended up to 1475 K in Figure 5, and the crystallization temperature T_m occurred at 1313 K in Figure 6. The melting enthalpy recovered between T_m and T_{n+} was the same all along the cycles from 2 to 21.

Figure 6 shows that $T_m = 1313$ K. The transition at T_{n+} during continuous cooling at 20 K/mn was no longer sharp and did not have a first-order character. Crystallization occurred at the melting temperature without undercooling, showing that the nuclei were growing between T_{n+} and T_m because they were formed above T_m by homogenous nucleation accompanied by an enthalpy increase. Phase 3 disappeared above T_{n+} and $\Delta\epsilon_{lg} = 0$. Crystallization was sharper and sharper during cycling from temperatures higher than T_{n+} , showing that the short-range order was enhanced. The enthalpy coefficient $\Delta\epsilon_{lg}$ of phase 3 grew by cooling below T_{n+} .

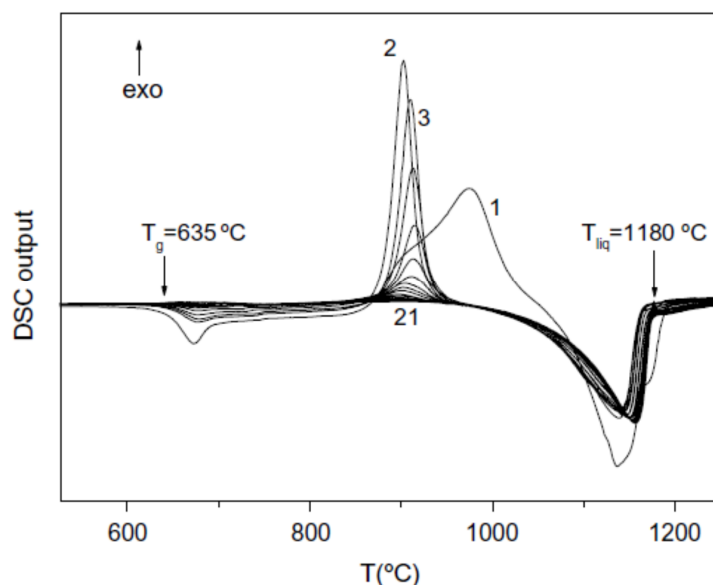


Figure 5. The repeated DSC up-scanning to 1250 °C ($T_{liq} + 70$ °C) at 0.333 K/s. The numerals next to the graphs represent the order of the DSC up-scans. The measurements are performed in argon at the heating rate 20 °C/min. Reprinted with permission from ref. [44], Figure 2, Copyright 2004 Elsevier.

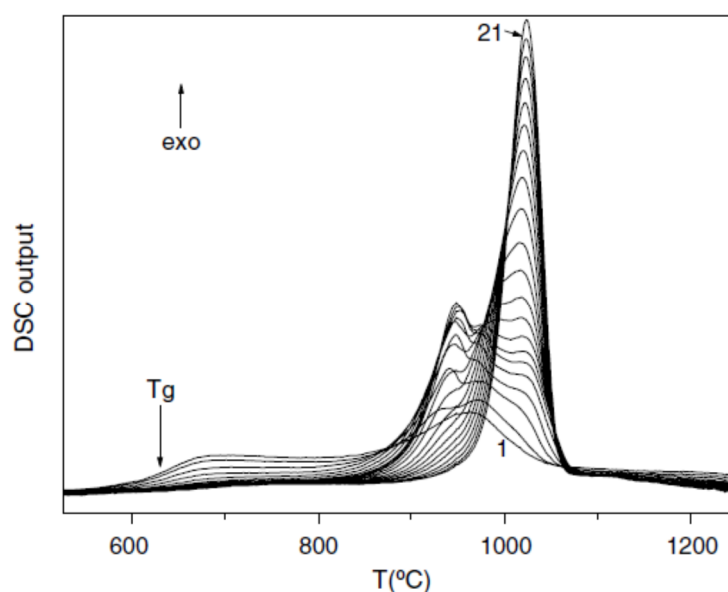


Figure 6. The repeated DSC down-scanning from 1250 °C ($T_{n+} + 70$ °C). The numerals next to the graphs represent the order of the DSC down-scans. The measurements are performed in argon at the cooling rate 20 °C/min. Reprinted with permission from ref. [44], Copyright Elsevier.

3.6. Endothermic Enthalpy Recovered at 1114 K in $Zr_{41.2}Ti_{13.8}Cu_{12.5}Ni_{10}Be_{22.5}$ (Vit1)

We follow data of ref. [45]. The glass transition occurred at $T_g = 625$ K and the melting temperatures at $T_{sol} = 965$ K and $T_{liq} = 1057$ K (Figure 7). There was an endothermic enthalpy at $T = 1114$ K. The heat capacity jump at T_g was $\Delta C_p(T_g) \cong 21.6$ J/K/g-atom. A heat capacity peak of superheated liquid after supercooling was observed during heating around $T = 1114$ K, accompanied by an endothermic latent heat of about 1100 J/mole. Another transition, observed by viscosity measurements, occurred at 1225 K by heating and subsequent cooling, showing that the liquid became homogeneous above this temperature [46].

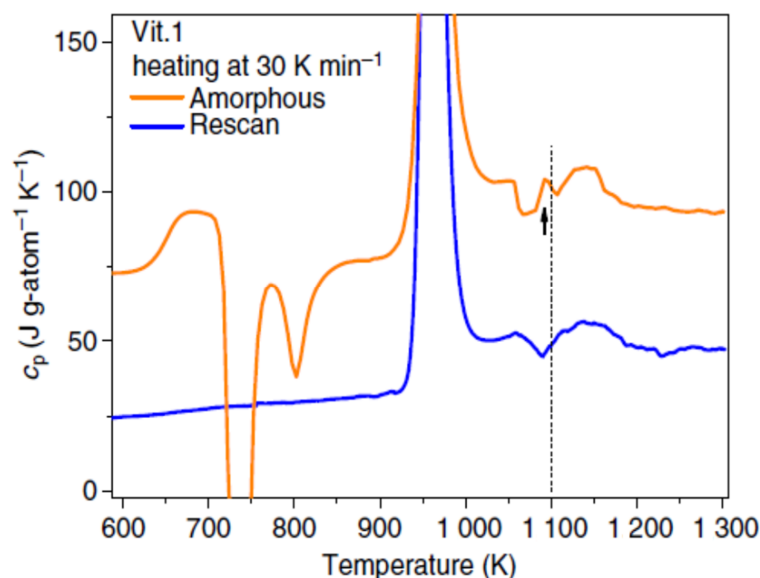


Figure 7. C_p measured upon heating at 30 K/min for the amorphous sample (upper) and once-melted crystallized sample (lower) (vertically shifted for clarity). Reprinted from ref. [45], Figure 1b.

Structural changes corresponding to these anomalies were still observed with in-situ synchrotron X-ray-scattering experiments in a contactless environment using an electrostatic levitator (ESL). There was an endothermic liquid–liquid transition at 1114 K during heating reinforced by the symmetrical observation of an exothermic latent heat regarding $T_m = 965$ K and an exothermic structural change around 816 K by supercooling.

3.7. Endothermic Enthalpy Recovered at 980–1000 K for $T_m = 876$ –881 K in PdNiP Liquid Alloys

The heat capacities of several PdNiP alloys measured at 20 K/min are represented in Figure 8. The melting temperatures were slowly varying with composition around 880 K and an enthalpy recovery temperature was still observed around 990 K in many liquid alloys. The theoretical predictions for these liquid alloys were limited to the case of $\text{Pd}_{42.5}\text{Ni}_{42.5}\text{P}_{15}$ [21] presented in Sections 6.1 and 7.1.

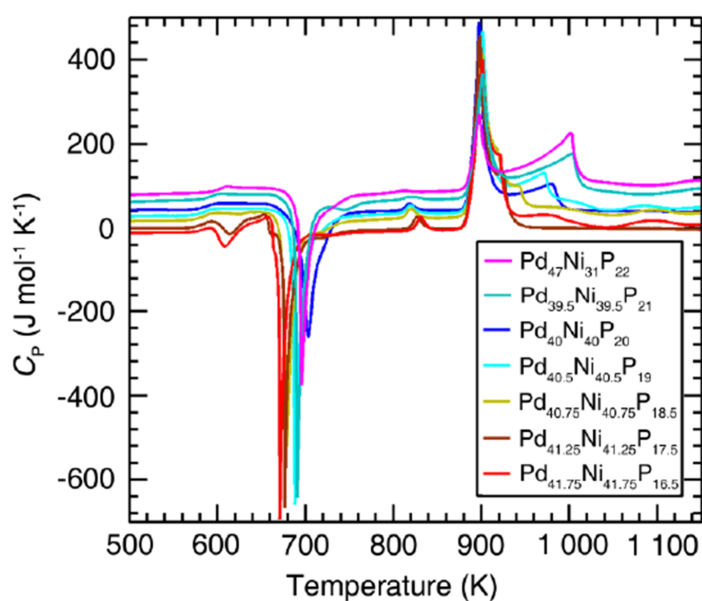


Figure 8. DSC data during heating for Pd-Ni-P metallic glasses. The heating rate is 20 K/min. The curves have been shifted vertically for clarity. Reprinted from ref. [47], Figure S3.

4. Predictions of Enthalpy Recovery Temperatures at $T_{n+} > T_m$

Equations (10)–(15) were used to calculate the enthalpy coefficients of fragile Liquids 1, 2, and 3 in Section 4.1, Section 4.2, Section 4.4, Section 4.5, and Section 4.6. Liquid $Ni_{77.5}B_{22.5}$ in 4.3 being strong, the enthalpy coefficients ϵ_{ls0} and ϵ_{gs0} were calculated with (9) for $\theta_{n-} = \theta_g$, $\theta_{0g}^2 = 1$ and $\theta_{0m}^2 = 4/9$.

4.1. Exothermic Enthalpy Delivered at $T_{n+} = 688$ K in $Al_{88}Ni_{10}Y_2$

We follow data of ref. [41]. The enthalpy coefficients of this fragile glass-forming melt were calculated with $T_g = 380$ K and $T_m = 602$ K:

$$\text{Liquid 1 : } \epsilon_{ls}(\theta) = 1.63123(1 - \theta^2/0.26736) \quad (17)$$

$$\text{Liquid 2 : } \epsilon_{gs}(\theta) = 1.44694(1 - \theta^2/0.3557) \quad (18)$$

$$\text{Liquid 3 : } \Delta\epsilon_{lg}(\theta) = 0.18439 - 2.05237 \times \theta^2 \quad (19)$$

The temperature $T_{n+} = 688$ K was deduced from $\theta_{n+} = \Delta\epsilon_{lg}(\theta_{n+}) = 0.14287$ [48]. In Figure 1, an exothermic enthalpy peak is observed at 688 K for all samples at 0.67 K/s.

4.2. Exothermic Enthalpy Delivered at $T_{n+} = 1622$ K in $(Fe_{71.2}B_{24}Y_{4.8})_{96}Nb_4$

We follow data of ref. [42]. The enthalpy coefficients of this fragile glass-forming melt were calculated with $T_g = 963$ K and $T_m = 1410$ K [48]:

$$\text{Liquid 1 : } \epsilon_{ls}(\theta) = 1.61206(1 - \theta^2/0.27795) \quad (20)$$

$$\text{Liquid 2 : } \epsilon_{gs}(\theta) = 1.41609(1 - \theta^2/0.36676) \quad (21)$$

$$\text{Liquid 3 : } \Delta\epsilon_{lg}(\theta) = 0.19397 - 1.93329 \times \theta^2 \quad (22)$$

The temperature $T_{n+} = 1622$ K was deduced from $\theta_{n+} = \Delta\epsilon_{lg}(\theta_{n+}) = 0.1503$ [48].

4.3. Exothermic Enthalpy Delivered at $T_{n+} = 1835$ K in $Ni_{77.5}B_{22.5}$

We follow data of ref. [24]. The enthalpy coefficients of this strong glass-forming melt were calculated with $T_g = 690$ K and $T_m = 1410$ K:

$$\text{Liquid 1 : } \epsilon_{ls}(\theta) = 1.09891(1 - \theta^2/0.44444), \quad (23)$$

$$\text{Liquid 2 : } \epsilon_{gs}(\theta) = 0.51347(1 - \theta^2) \quad (24)$$

$$\text{Liquid 3 : } \Delta\epsilon_{lg}(\theta) = 0.58553 - 1.958 \times \theta^2 \quad (25)$$

The temperature $T_{n+} = 1835$ K was deduced from $\theta_{n+} = \Delta\epsilon_{lg}(\theta_{n+}) = 0.34808$ [48] in agreement with Figure 3.

4.4. Exothermic Enthalpy Delivered at $T_{n+} = 1356$ K in $Cu_{47.5}Zr_{45.1}Al_{7.4}$

We follow data of ref. [43]. The enthalpy coefficients of this fragile glass-forming melt were calculated from $T_g = 690$ K and $T_m = 1170$ K:

$$\text{Liquid 1 : } \epsilon_{ls}(\theta) = 1.5906(1 - \theta^2/0.28942) \quad (26)$$

$$\text{Liquid 2 : } \epsilon_{gs}(\theta) = 1.3859(1 - \theta^2/0.37826) \quad (27)$$

$$\text{Liquid 3 : } \epsilon_{lg}(\theta) = 0.2047 - 1.83194 \times \theta^2 \quad (28)$$

The temperature $T_{n+} = 1356$ K and the recovered enthalpy coefficient $\Delta\epsilon_{lg}$ were deduced from $\theta_{n+} = \Delta\epsilon_{lg}(\theta_{n+}) = 0.1586$ [48] in agreement with Figure 4. The enthalpy

coefficient $\Delta\epsilon_{lg}$ reappeared by homogeneous nucleation below T_{n+} because $\epsilon_{gs}(\theta_{n+})$ was weaker than $\epsilon_{ls}(\theta_{n+})$ and liquid 1 enthalpy decreased toward that of liquid 2 at slow cooling.

4.5. Endothermic Enthalpy Recovered at $T_{n+} = 1470$ K in a Silicate Liquid

We follow data of ref. [44]. The enthalpy coefficients of this fragile glass-forming melt were calculated with $T_g = 908$ K and $T_m = 1313$ K:

$$\text{Liquid 1 : } \epsilon_{ls}(\theta) = 1.69155(1 - \theta^2/0.23189) \quad (29)$$

$$\text{Liquid 2 : } \epsilon_{gs}(\theta) = 1.53732(1 - \theta^2/0.31613) \quad (30)$$

$$\text{Phase 3 : } \Delta\epsilon_{lg}(\theta) = 0.15473 - 2.4315 \times \theta^2 \quad (31)$$

The temperature $T_{n+} = 1470$ K was deduced from $\theta_{n+} = \Delta\epsilon_{lg}(\theta_{n+}) = 0.1195$ [48] in agreement with Figure 5.

4.6. Endothermic Enthalpy Recovered at $T_{n+} = 1114$ K in $Zr_{41.2}Ti_{13.8}Cu_{12.5}Ni_{10}Be_{22.5}$ (Vit1)

We follow data of ref. [45]. The enthalpy coefficients of this fragile glass-forming melt were calculated with $T_g = 625$ K and $T_m = 965$ K [35]:

$$\epsilon_{ls} = 1.70651 \times (1 - \theta^2/0.2226) \quad (32)$$

$$\epsilon_{gs} = 1.4715 \times (1 - \theta^2/0.34564) \quad (33)$$

$$\Delta\epsilon_{lg} = 0.23501 - 3.409 \times \theta^2. \quad (34)$$

The temperature $T_{n+} = 1114$ K was deduced from $\theta_{n+} = \Delta\epsilon_{lg}(\theta_{n+}) = 0.15407$ [48] in agreement with Figure 6. The observed double transition was the consequence of the presence in the melt of nuclei, all having the same Gibbs free energy, leading to a homogenous nucleation at 818 and 1114 K as consequence of the quadratic equation of $\Delta\epsilon_{lg}(\theta_{n+}) = \theta_{n+}$. The ordered liquid was rebuilt at $T_{n+} = 818$ K during cooling from 1350 K with the formation in the no-man's land of new superclusters, building a vitreous solid phase at T_g resulting of the bond number divergence. The hysteresis of viscosity disappeared at about 1225 K when the liquid is homogeneous [46]. A "colloidal" state was melted above the temperature of viscosity or density branching observed during cooling after heating [24,26,27,46]. Equation (35) was used to calculate the reduced temperature θ_{n+} of glass-forming melt with a glass transition at θ_g and obeying (11) with $a = 1$ [48]:

$$\theta_{n+} = -0.38742 \times \theta_g \quad (35)$$

The liquidus melting temperature $T_{liq} = 1057.5$ K was deduced from Equation (35) with $T_g = 625$ K and $T_{n+} = 1225$ K in perfect agreement with the experimental observation of liquidus presented in Figure 7. This finding of a second transition above T_{n+} agreed with the first-order liquid-liquid transitions observed above T_{n+} in $Pd_{42.5}Ni_{42.5}P_{15}$ and $La_{50}Al_{35}Ni_{15}$.

5. Three Liquid States above the Melting Temperature

The exothermic and endothermic transitions at T_{n+} led to a liquid above T_{n+} with an enthalpy coefficient $\Delta\epsilon_{lg} = 0$. Two other liquid states existed at T_m with enthalpy coefficients equal to $\pm\Delta\epsilon_{lg0}$. The melting temperature T_m was chosen equal to $T_{solidus}$ in Figure 9. The enthalpy coefficients ($\pm\Delta\epsilon_{lg}$), defined by (15) and applied to $Pd_{42.5}Ni_{42.5}P_{15}$ in Figure 9 and in Section 7.1, were related to the enthalpy decrease and increase with temperature of these two quenched liquid states toward that of homogeneous liquid.

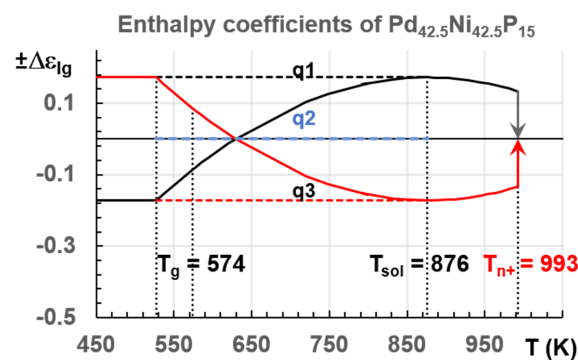


Figure 9. The enthalpy coefficients of $\text{Pd}_{42.5}\text{Ni}_{42.5}\text{P}_{15}$ versus T (K). $T_{n+} = 993$ K; $T_{\text{solidus}} = 876$ K; $T_g = 574$ K; $T_3 = 527.3$ K. The enthalpy coefficients ($\pm\Delta\varepsilon_{lg}$) given by (15) versus T (K). Three quenching lines q1, q2, and q3 along $+\Delta\varepsilon_{lg0} = 0.17237$, 0 , and $-\Delta\varepsilon_{lg0}$.

The homogeneous liquid can be quenched along q2 ($\Delta\varepsilon_{lg0} = 0$) in Figure 9 from above the temperature where the liquid became homogeneous, down to temperatures much weaker than T_g [49–51]. An enthalpy relaxation at low heating rate, equal to $(-\Delta\varepsilon_{lg0} \times \Delta H_m)$, built the bonds of phase 3 and led by heating to the temperature where $\Delta\varepsilon_{lg} = 0$ [35]. This slow heating through T_g broke the bonds and the liquid enthalpy increases up to $(+\Delta\varepsilon_{lg0} \times \Delta H_m)$ at T_m , producing an exothermic enthalpy at T_{n+} . These phenomena are observed in Figures 1–4.

With a much higher heating rate, the enthalpy of bonds, building phase 3, did not have the time to relax below T_g , and phase 3 was not formed along the thermal path below T_g and the latent heat at T_{n+} was not observed for $\text{Pd}_{42.5}\text{Ni}_{42.5}\text{P}_{15}$ at 100 K/s, as shown in Figure 10 [21]. The liquid being frozen below T_g with $\Delta\varepsilon_{lg} = 0$ gave rise to an endothermic enthalpy at T_g due to bond breaking and the liquid returned to a homogeneous state with $\Delta\varepsilon_{lg0} = 0$ above T_{n+} [10–12].

A quench along q1 in Figure 9 from $T_m < T < T_{n+}$ with a liquid enthalpy $(+\Delta\varepsilon_{lg0} \times \Delta H_m)$ at T_m led to an amorphous phase with an enthalpy excess $(+\Delta\varepsilon_{lg0} \times \Delta H_m)$. Phase 3 bonds were built during reheating and they decreased, at a low heating rate, the enthalpy coefficient from $(+\Delta\varepsilon_{lg0})$ below T_g to $(-\Delta\varepsilon_{lg0})$ at T_m , leading to an endothermic latent heat at T_{n+} corresponding to crystallized nuclei melting at T_{n+} .

Starting heating at a very low heating rate from any liquid state led to crystallization and to a liquid enthalpy equal to $(-\Delta\varepsilon_{lg0} \times \Delta H_m)$ at T_m .

A quench from $T_m < T < T_{n+}$ along q3 led to the enthalpy of phase 3 with crystallized nuclei being the skeleton of this phase after percolation at T_g , as shown for plastic crystals. A slow cooling led to crystallization at T_m without undercooling [19].

The endothermic and exothermic characters of the transition at T_{n+} were imposed by the initial value of the liquid enthalpy after quenching and by cooling and heating rates.

Homogeneous nucleation in the liquid was expected to depend on the time of aging in the range of temperatures below and close to the homogenization temperature. The first-order liquid–liquid transitions in $\text{Pd}_{42.5}\text{Ni}_{42.5}\text{P}_{15}$ and $\text{La}_{50}\text{Al}_{35}\text{Ni}_{15}$ studied by [20,21] combined with our non-classical model of homogeneous nucleation shed light on these new phenomena.

6. First-Order Liquid–Liquid Transitions Observed in $\text{Pd}_{42.5}\text{Ni}_{42.5}\text{P}_{15}$, $\text{La}_{50}\text{Al}_{35}\text{Ni}_{15}$, and Fe_2B

We follow data of ref. [21] for $\text{Pd}_{42.5}\text{Ni}_{42.5}\text{P}_{15}$, of ref. [20] for $\text{La}_{50}\text{Al}_{35}\text{Ni}_{15}$ and of ref. [24] for Fe_2B .

6.1. $\text{Pd}_{42.5}\text{Ni}_{42.5}\text{P}_{15}$

6.1.1. Fast Differential Scanning Calorimetry at 100 K/s

The fast differential scanning calorimetry (FDSC) heating curve at 100 K/s represented in Figure 10 and reproduced from [21] was used to determine the solidus and liquidus

temperatures $T_{\text{sol}} = 876$ and $T_{\text{liq}} = 926.5$ K. A first-order liquid–liquid transition was observed at $T_{\text{LL}} = 1063$ K. The sample was previously cooled from 1073 K at 40,000 K/s down to room temperature and reheated up to 1073 K, which was a temperature higher than the first-order transition observed at T_{LL} .

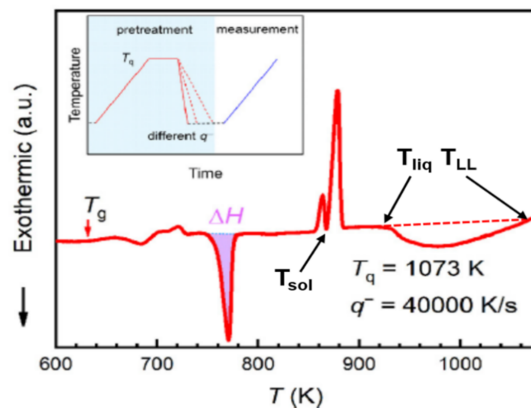


Figure 10. DSC with heating rate of 100 K/s. A typical FDSC heating curve of the sample obtained from $T_q = 1073$ K and $q^- = 40,000$ K/s. The enthalpy of crystallization is denoted as ΔH . The inset shows the temperature protocol of the FDSC experiments. Temperatures T_{sol} , T_{liq} , and T_{LL} added. Reprinted with permission from ref. [21], Figure 3a, Copyright 2021 Elsevier.

6.1.2. Melting Transition Observed at 993 K above the Solidus Temperature $T_{\text{sol}} = 876$ K of $\text{Pd}_{42.5}\text{Ni}_{42.5}\text{P}_{15}$

The samples were quenched from T_q to room temperature at a cooling rate of $q^- = 40,000$ K/s and reheated at 100 K/s up to T_q , as shown in Figure 11b [21]. There was no nucleation when cooling started from 1073 K for $q > 70$ K/s, while crystallization occurred for $q < 7000$ K/s when cooling started from 1023 K as shown in Figure 11a. The area of the crystallization peak occurring around $T = 770$ K in Figure 10 was plotted versus T_q in Figure 11b. The temperature $T = 993$ K was viewed by the authors as a liquidus temperature which was, in fact, equal to 926.5 K, as shown in Figure 9.

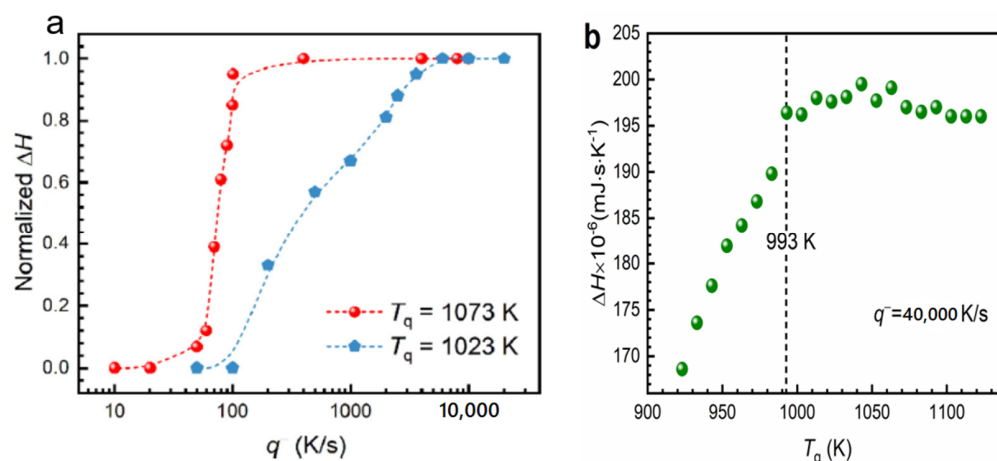


Figure 11. The content of amorphous phase as a function of cooling rate q^- of the samples obtained from $T_q = 1073$ and 1023 K, respectively (a). The crystallized fraction characterized by ΔH is evaluated by FDSC as shown in Figure 10b. Area of the second exothermic peak ΔH as a function of T_q as shown in Figure 10. (b) Area of the exothermic peak ΔH as a function of T_q with a cooling rate of 40,000 K/s. Reprinted with permission from ref. [21], Figure 3b and Figure S1, Copyright 2021 Elsevier.

6.1.3. First-Order Transition Observed by ^{31}P Nuclear Magnetic Resonance (NMR)

^{31}P NMR was used to characterize the LLT at $T_{\text{LL}} = 1063\text{ K}$ above $T_{\text{n}+} = 993\text{ K}$. The liquid alloy was first heated to 1293 K for homogenization during 30 min , and then cooled step by step to 1043 K . NMR spectra were taken isothermally after equilibrating the liquid at 1293 K at each step. The Knight shift (K_s) was determined by the ensemble average of local magnetic field around ^{31}P nuclei, sensitive to the changes in structure, plotted in Figure 12 as a function of temperature [21]. (K_s) varied linearly above 1063 K with a slope increase of 1.76 ppm/K below 1063 K , indicating a change in the P-centered local structures at this temperature. This change was viewed as a first-order liquid–liquid transition (LLT) analogous to that observed in $\text{La}_{50}\text{Al}_{35}\text{Ni}_{15}$ where a second change of K_s in this new liquid state was observed at lower temperatures attributed to the hysteresis of the transition [20].

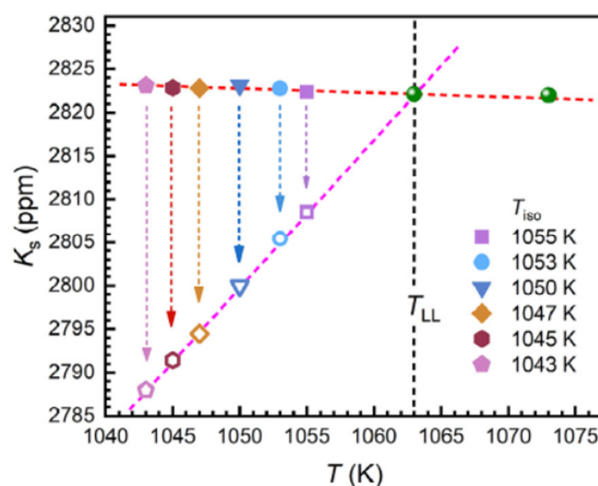


Figure 12. The changes of the Knight shift K_s at different undercooled temperatures T_{iso} after quenching the melt from 1173 K . The solid and open symbols represent the initial and equilibrium K_s , respectively. Reprinted with permission from ref. [21], Figure 1c, Copyright 2021 Elsevier.

6.2. $\text{La}_{50}\text{Al}_{35}\text{Ni}_{15}$

This melt was characterized by $T_g = 528\text{ K}$, $T_{\text{sol}} = 877.6\text{ K}$, and $T_{\text{liq}} = 892\text{ K}$, as shown in Figure 13 ([20] Figure S1). A second liquidus temperature was found at 950 K . The temperature T_{LL} , observed at 1033 K by measuring the ^{27}Al Knight shift by RMN, is viewed as a first-order LLT in Figure 14. A phenomenon analogous to hysteresis led to a second transition at 1013 K .

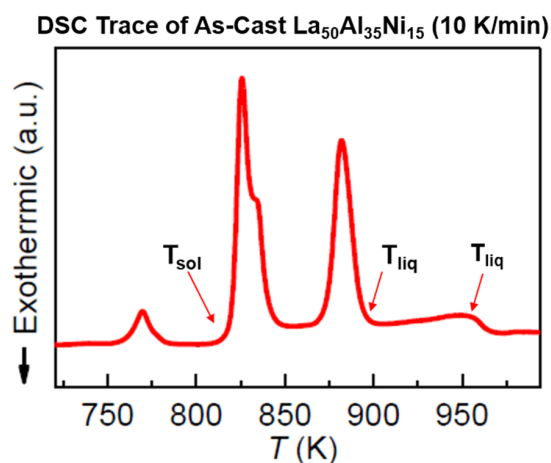


Figure 13. DSC trace of as-cast $\text{La}_{50}\text{Al}_{35}\text{Ni}_{15}$ BMG. The DSC curve obtained at a heating rate of 10 K/min . Liquidus temperature (T_{liq}) indicated by red arrows. The two liquidus temperatures ($T_{\text{n}+}$) and solidus temperature (T_{sol}) are added. Reprinted from ref. [20], Figure S1.

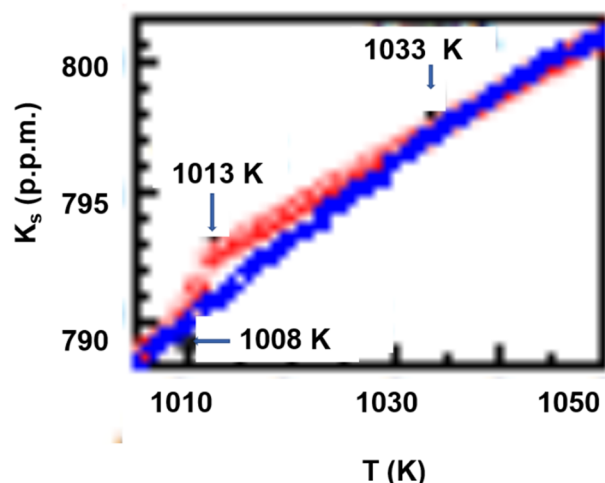


Figure 14. Temperature dependence of ^{27}Al knight shift K_s during continuous cooling and reheating in the temperature interval of 973–1143 K. The upper red dashed line represents the fitting curves of K_s versus T with a slope of 0.22 ppm/K and the lowest blue dashed line represents the fitting curve with a slope of 0.33 p.p.m./K. The two fitting curves intersect at 1033 K. Three characteristic temperatures indicated by black arrows 1033, 1013, and 1008 K. Reprinted from ref. [20], Figure 1b.

6.3. Fe_2B

The vitreous state of this compound was obtained by mechanical alloying [52]. The first-order transition occurs at $T_{\text{LL}} = 1915$ K in Figure 15 with a melting temperature of 1662 K [24].

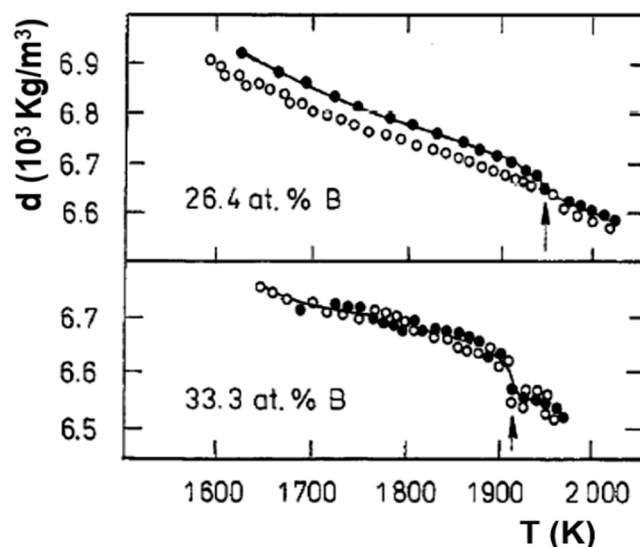


Figure 15. Temperature dependence of the density d of Fe-26.4 at.%B and Fe-33.3 at.%B melts at heating after melting (\bullet) and subsequent cooling (\circ). Arrow shows the anomaly linked with structural transformation in a liquid compound. Reprinted with permission from ref. [24], Figure 8, Copyright 1997 Elsevier.

7. Predictions of First-Order Transition Temperatures by Homogenous Nucleation in $\text{Pd}_{42.5}\text{Ni}_{42.5}\text{P}_{15}$, $\text{La}_{50}\text{Al}_{35}\text{Ni}_{15}$ and Fe_2B Melts

These first-order transitions were observed at T_{LL} at very low cooling rates or by isothermal annealing between the melting temperature and T_{LL} . The homogeneous liquid state characterized by $\Delta\varepsilon_{\text{lg}0} = 0$ was stable during cooling in Figure 3 while the first-order transitions were reversible in Figure 15. The two melting temperatures T_{sol} and T_{liq} of non-congruent materials led to two nucleation temperatures $T_{\text{n}+}$.

7.1. Predictions of Transitions in $Pd_{42.5}Ni_{42.5}P_{15}$ Melt

The temperature 993 K in Figure 11b was viewed by [21] as a liquidus temperature which was, in fact, equal to 926.5 K, as shown in Figure 10. The reduction of the enthalpy recovered by crystallization at 770 K occurred for $T_q < 993$ K, as shown in Figure 11b. The crystallization enthalpy at 770 K was continuously reduced without exothermic enthalpy jump equal $0.13357 \times 197 = 26$ in Figure 11b at 993 K. The mean-range order accompanied by exothermic enthalpy progressively reappeared by homogeneous nucleation in the liquid heated during 30 s at each temperature T_q and was completely formed at $T_{liq} = 926.5$ K because the enthalpy decrease was equal to -13.4% at this temperature. The residual configurons melted at $T_{n+} = 993$ K using (35) ($\theta_{n+} = \Delta\varepsilon_{lg}(\theta_{n+}) = 0.13357$), $T_m = 876$ K, and $T_g = 574$ K. This value of T_g agreed with measurements of heat capacity of melts with similar compositions [47]. The enthalpy coefficients of $Pd_{42.5}Ni_{42.5}P_{15}$ for the liquidus and solidus liquid states were given in Equations (36–38) using Equations (10–16):

For $T_{sol} = 876$ K and $T_g = 574$ K

$$\text{Liquid 1 : } \varepsilon_{ls}(\theta) = 1.65525(1 - \theta^2/0.25362) \quad (36)$$

$$\text{Liquid 2 : } \varepsilon_{gs}(\theta) = 1.48288(1 - \theta^2/0.34081) \quad (37)$$

$$\text{Phase 3 : } \Delta\varepsilon_{lg}(\theta) = 0.17237 - 2.1755 \times \theta^2 \quad (38)$$

For $T_{Liq} = 926.45$ K and $T_g = 574$ K

$$\text{Liquid 1 : } \varepsilon_{ls}(\theta) = 1.61957(1 - \theta^2/0.27384) \quad (39)$$

$$\text{Liquid 2 : } \varepsilon_{gs}(\theta) = 1.42935(1 - \theta^2/0.36251) \quad (40)$$

$$\text{Phase 3 : } \Delta\varepsilon_{lg}(\theta) = 0.19022 - 1.97146 \times \theta^2 \quad (41)$$

Applying Equation (35) led to $T_{n+} = T_{LL} = 1063$ K in perfect agreement with Figure 12. From our analysis, a second change of K_s occurred by homogeneous nucleation in $Pd_{42.5}Ni_{42.5}P_{15}$ at $T_{n+} = 993$ K. This transition was not only due to the hysteresis of a first-order transition because there were two homogeneous nucleation temperatures as shown in Figure 12. This point was still confirmed in 7.2 devoted to $La_{50}Al_{35}Ni_{15}$, where the changes of K_s occurred for two values of T_{n+} because there were, in these non-congruent liquid compounds, two solid–liquid transitions characterized by solidus and liquidus temperatures.

The temperature $T_{n+} = T_{LL} = 1063$ K corresponded to the temperature of homogeneous nucleation of colloids containing critical numbers n_c of atoms with n_c given by Equation (42) (see [9], Equation (48)):

$$n_c = \frac{8N_A k_B (1 + \Delta\varepsilon_{lg})^3}{27\Delta S_m (\Delta\varepsilon_{lg})^3} \ln(K) \quad (42)$$

where N_A is the Avogadro number, k_B the Boltzmann constant, ΔS_m the melting entropy, and $\ln K \cong 90$ [5]. With $\Delta\varepsilon_{lg} = 0.13356$ and $\Delta S_m = 8.76$ J/g-atom [47], $n_c = 15522$ at the temperature $T_{n+} = 993$ K. With $\Delta\varepsilon_{lg} = 0.14739$ and $\Delta S_m = 8.76$ J/g-atom, $n_c = 11977$ at the temperature $T_{n+} = 1063$ K. Critical numbers n_c , still larger, were observed in Pb–Bi liquid alloys below the temperature of liquid homogenization [27]. The number of atoms inside an elementary superatom in the homogeneous liquid above 1063 K was equal to 135, with $\Delta\varepsilon_{lg}(\theta_{n+})$ replaced in (42) by $\varepsilon_{gs}(\theta_{n+}) = 1.40526$ in (42) using Equations (39) and (40). The homogeneous nucleation time τ (s) for temperatures $1043 < T < 1063$ K was following Equation (43) (see Figure 1d in ref. [21]):

$$\tau(s) = 5.9 \times 10^{-3} \left(\frac{1063}{T} - 1 \right)^{2.18} \quad (43)$$

which led by extrapolation to $\tau \cong 1.9$ s at $T_{n+} = 993$ K.

There was no growth nucleus inducing crystallization after quenching from the temperature $T = 1073$ K which was higher than $T_{LL} = 1063$ K as shown in Figure 11a [21]. New growth nuclei were added when the melt was quenched from 1023 K, a temperature higher than $T_{n+} = 993$ K and much higher than T_{sol} . Consequently, new denser nuclei growing from the colloidal state were added by homogeneous nucleation at 1023 K above 993 K. The transition at 993 K after cooling from 1073 K was due to the internal and external bond formation between colloids below 1063 K [18]. This observation agreed with the growth of n_c from 11977 to 15522 between 1063 and 993 K. The transitions observed by NMR below 1063 K involved all ^{31}P atoms and corresponded to the colloid formation through the relaxation time decrease [23]. The first-order character of this transition was observed at each step of isothermal annealing below 1063 K. The breaking of bonds inside and outside colloids occurred at the lowest temperature T_{n+} during heating [18], while at the highest T_{n+} , a transition from colloidal state to a new homogeneous state made of elementary superatoms only organized by short-range order appeared.

The enthalpy coefficients ($-\Delta\varepsilon_{lg0}$) of phase 3 equal to those of configurons are represented in Figure 16 as a function of the temperature T (K) for T_{sol} and T_{liq} using Equations (38) and (41). The crystallization temperature occurred at the reentrant formation temperature of ultrastable glass with its enthalpy equal to $-\Delta\varepsilon_{lg0}$. This nucleation temperature opened the door to crystallization [19].

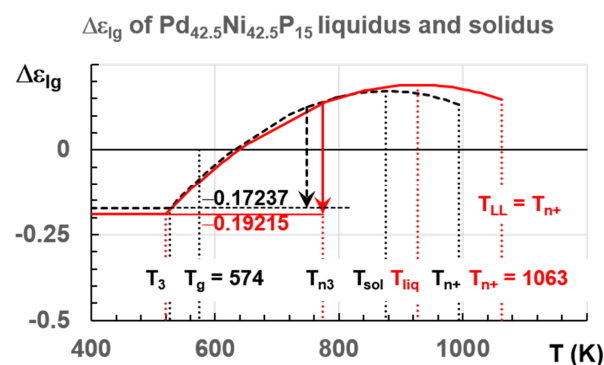


Figure 16. Enthalpy coefficients of liquidus and solidus melts versus T (K). $T_{liq} = 926.5$ K, $T_{n+} = 1063$ K, $T_{sol} = 876$ K, and its $T_{n+} = 993$ K. Crystallization at the nucleation temperature $T_3 = 748.4$ K of phase 3 in solidus melt instead of $T_3 = 774.2$ K in liquidus melt. In the liquidus melt, $T_{LL} = T_{n+} = 1063$ K.

7.2. Predictions of First-Order Transitions in $\text{La}_{50}\text{Al}_{35}\text{Ni}_{15}$ Glass-Forming Melt

We follow data of ref. [20]. The phase 3 enthalpy coefficients of $\text{La}_{50}\text{Al}_{35}\text{Ni}_{15}$ for the liquidus and solidus liquids were given in Equations (44)–(49) for $T_{sol} = 877.6$ K, $T_{liq} = 892$ K, and $T_g = 528$ K, and are represented in Figure 17.

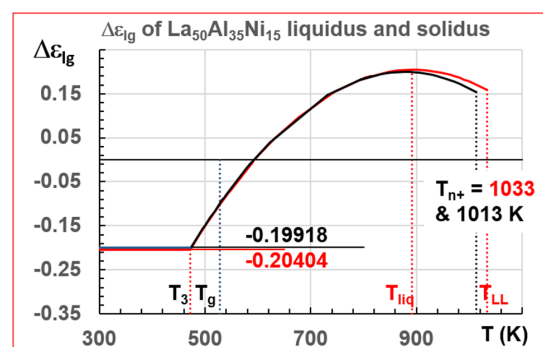


Figure 17. $\text{La}_{50}\text{Al}_{35}\text{Ni}_{15}$ enthalpy coefficients of liquidus and solidus melts. $T_{sol} = 877.6$ K; $T_{n+} = 1013$ K; $T_{liq} = 892$ K; $T_{n+} = T_{LL} = 1033$ K. The enthalpy coefficients of ultrastable phase 3 are (-0.19918) for the solidus and (-0.20404) for the liquidus. The two melts have the same $T_g = 574$ K.

For $T_{\text{Liq}} = 892$ and $T_g = 528$ K:

$$\text{Liquid 1 : } \varepsilon_{\text{ls}}(\theta) = 1.66143(1 - \theta^2/0.25000) \quad (44)$$

$$\text{Liquid 2 : } \varepsilon_{\text{gs}}(\theta) = 1.42935(1 - \theta^2/0.33679) \quad (45)$$

$$\text{Phase 3 : } \Delta\varepsilon_{\text{lg}}(\theta) = 0.20404 - 2.2516 \times \theta^2 \quad (46)$$

For $T_{\text{sol}} = 877.6$ and $T_g = 528$ K:

$$\text{Liquid 1 : } \varepsilon_{\text{ls}}(\theta) = 1.60164(1 - \theta^2/0.28357) \quad (47)$$

$$\text{Liquid 2 : } \varepsilon_{\text{gs}}(\theta) = 1.40246(1 - \theta^2/0.37246) \quad (48)$$

$$\text{Phase 3 : } \Delta\varepsilon_{\text{lg}}(\theta) = 0.19218 - 1.88273 \times \theta^2 \quad (49)$$

7.3. Predictions of Glass Transition Temperature of Fe_2B Melt

The enthalpy coefficients of the strong liquid Fe_2B were calculated with Equations (9) and (35), $T_m = 1662$ K and $T_{n+} = T_{\text{LL}} = 1915$ K, given in Equations (50)–(52). Phase 3 is represented in Figure 18.

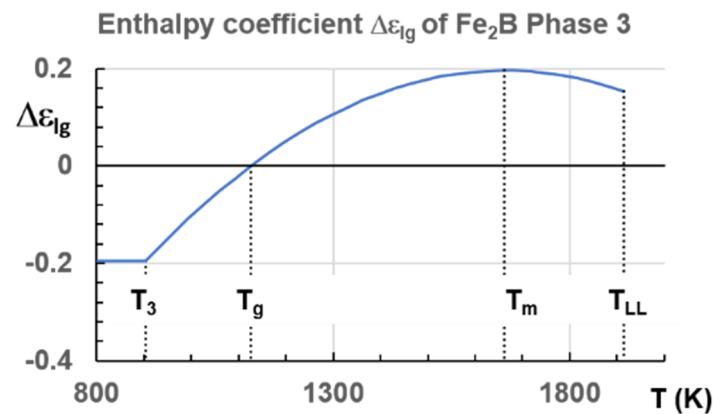


Figure 18. Enthalpy coefficient $\Delta\varepsilon_{\text{lg}}(T)$ of Fe_2B Phase 3 and configurons. $T_3 = 903$ K, $T_g = 1125.7$ K, $T_m = 1662$ K, $T_{n+} = T_{\text{LL}} = 1915$ K.

For $T_m = 1662$ K and $T_{n+} = T_{\text{LL}} = 1915$ K, $T_g = 1125.7$ K:

$$\text{Liquid 1 : } \varepsilon_{\text{ls}}(\theta) = 1.60164(1 - \theta^2 \times 2.25) \quad (50)$$

$$\text{Liquid 2 : } \varepsilon_{\text{gs}}(\theta) = 1.1519(1 - \theta^2) \quad (51)$$

$$\text{Phase 3 : } \Delta\varepsilon_{\text{lg}}(\theta) = 0.19579 - 1.8804 \times \theta^2 \quad (52)$$

7.4. One Liquid–Liquid Transition at $T_{n+} = T_{\text{LL}}$ in Congruent Materials and Two in the Others

A first-order transition occurred at T_{LL} due to the formation by cooling of colloidal state assembling elementary superatoms composed of tenths atoms bounded by short-range interactions, leading to colloids containing thousands of atoms. In the case of congruent materials, only one liquid–liquid transition was expected. The lowest and the highest temperatures T_{n+} were equal and T_{n+} is a first-order transition temperature equal to T_{LL} . This is the case for Fe_2B .

These colloids were similar atom clouds containing a magic atom number of atoms because they were melted by homogeneous nucleation instead of surface melting. They

had a maximum radius for which their Gibbs free energy was smaller or equal to that of the melt [53].

There were two liquid–liquid transitions above the solidus and liquidus temperatures T_{sol} and T_{liq} in non-congruent materials, leading to two temperatures T_{n+} . The highest one was equal to T_{LL} and related to T_{liq} . Above T_{LL} , the liquid was homogeneous and atoms were only submitted to short-range order in tiny superatoms. The lowest (T_{n+}) was related to T_{sol} and was the temperature where coupling between elementary superatoms started during cooling and led to bond percolation at T_g . The lowest one was a second-order phase transition where the residual configurations were melted during heating, involving 15% of the sample volume.

A melt was only rejuvenated above T_{n+} because all colloids and superatoms were disconnected.

8. Perspectives: Mpemba Effect and Bonding-Antibonding of Superatoms

8.1. Mpemba Effect and Its Inverse Relation to the Existence of Three Liquid States above the Melting Temperature

The Mpemba effect is described by a shorter time needed to crystallize a hot water system than to crystallize the same colder water system cooled down from initial lower temperatures [54]. This phenomenon was documented by Aristotle 2300 years ago [55]. The melting enthalpy of ice was $\Delta H_m = 334 \text{ J/g}$ with a specific heat of 4.18 J/g . Starting from a hot homogenous water, the exothermic enthalpy of formation of mean-range order below $T_{n+} = 295.3 \text{ K}$ ($22.1 \text{ }^\circ\text{C}$) [34] was progressively equal to $-0.0818 \times 334 = -27.3 \text{ J/g}$ by homogenous nucleation during slow cooling through T_{n+} . The value of T_{n+} in water was confirmed by numerical simulations of the melting temperature of an ultrathin layer of hexagonal ice [19,56–58]. The water enthalpy variation being equal to 92 J/g from 22.1 to $0 \text{ }^\circ\text{C}$, the temperature of $0 \text{ }^\circ\text{C}$ was quickly attained by the hot system because of the recovery of exothermic enthalpy. The cold water had no more available exothermic enthalpy because the formation of mean range order was much older in this water. Cooling this liquid took much more time.

The latent heat, expected at $T_{n+} = 22.1 \text{ }^\circ\text{C}$, was not observed up to now, while Mpemba and Osborne observed this effect with a slow cooling rate of 0.01 K/s . The window of nucleation was very narrow in congruent materials because the temperature T_{n+} was unique instead of extending between the two T_{n+} temperatures of non-congruent substances as shown in Figure 13. At a too-high cooling rate, the liquid state, with $\Delta\epsilon_{\text{lg}} = 0$, free of any growth nucleus, remained stable and showed undercooling. The homogeneous liquid state was stable when it escaped the formation of colloidal state at T_{n+} . Figure 3 showed this phenomenon in $\text{Fe}_{77.5}\text{B}_{22.5}$. On the contrary, the transition of Fe_2B at $T_{n+} = 1915 \text{ K}$ had a first-order character (see Figure 15) Nucleus formation started from the colloidal state and was expected to be formed at a low cooling rate.

Using the theory of nonequilibrium thermodynamics, Lu and Raz predicted a similar anomalous behavior with heating using a three-state model that we had here for all melts [59]. A cold liquid, with an enthalpy equal to $(+\Delta\epsilon_{\text{lg}0} \times \Delta H_m)$, obtained after building bonds below T_g , would develop an exothermic latent heat at T_{n+} during heating, while a warmer liquid with an enthalpy equal to $(-\Delta\epsilon_{\text{lg}0} \times \Delta H_m)$ would need an endothermic enthalpy to melt its mean-range order.

The Mpemba effect and its inverse effect can be extended to many systems [59,60] and we showed that these phenomena could exist in all melts. Moreover, we assumed that analogues of Mpemba effects should occur on vitrification of liquids so that glasses would be formed quicker out of hot melts compared with melts cooled down from lower temperatures. All these new events were observable because the transition at T_{n+} was a first-order transition in congruent materials [24].

8.2. Three Liquid States Associated with Bonding–Antibonding of Superatoms

In Figure 9, the enthalpy coefficient of phase 3 at T_{n+} was equal to three values $+\Delta\varepsilon_{lg}$, 0, and $-\Delta\varepsilon_{lg}$ depending on thermal history leading to three liquid states. The glass transitions occurred at the percolation threshold of superclusters, built by homogeneous nucleation, during the first cooling of liquids initially homogeneous. These superclusters survive in overheated colloids after their formation during the first cooling because they were melted at T_{n+} by homogeneous nucleation instead of surface melting at T_m . These entities were contained in colloids with a magic atom number [61]. Thus, they were melted at T_{n+} when their Gibbs free energy became equal to that of homogeneous liquid [53]. The endothermic and exothermic latent heats revealed the existence of two families of bound molecules which could be attributed to bonding and antibonding of colloids through elementary superatoms. This concept of bonding and antibonding is highly developed in bond chemistry to create new chemical structures. Bonding and antibonding of colloids could lead to higher and lower enthalpies. Two recent examples of research in this field were given [62,63]. The nature built these new superstructures in all overheated melts by homogeneous nucleation. The percolation of these superatoms led T_g to a superstructure involving 3D space in 15% of atoms [18].

9. Conclusions

Our models of homogeneous nucleation and configurons explained the formation of liquid phases above T_g with mean-range order disappearing at a temperature T_{n+} much higher than the melting temperature. This transformation at T_{n+} was a first-order transition in congruent materials such as Fe_2B and was expected to be observable at a very low cooling rate or by homogeneous nucleation during isotherm annealing below T_{n+} . There were two melting temperatures in non-congruent materials called solidus and liquidus temperatures, leading to two temperatures: T_{n+} starting with a unique glass transition temperature T_g . The first-order liquid–liquid transitions in $Pd_{42.5}Ni_{42.5}P_{15}$ and $La_{50}Al_{35}Ni_{15}$ observed with NMR at $T_{LL} = 1063$ and 1033 K, respectively, occurred at the temperature T_{n+} corresponding to the liquidus temperature of these two alloys. The two other second-order phase transitions, occurring at $T_{n+} = 993$ and 1013 K respectively, were induced by the solidus temperatures.

The latent heats produced at T_{n+} were exothermic or endothermic. We attributed this phenomenon to the presence of three liquid states at T_{n+} , with three enthalpy coefficients depending on the cooling rate and on the starting temperature of quenching. These enthalpies were equal to 0, $+\Delta H_m \times \Delta\varepsilon_{lg}(T_{n+})$, and $-\Delta H_m \times \Delta\varepsilon_{lg}$ in comparison with that of a homogeneous liquid equal to zero at high temperatures. These liquids, when quenched to temperatures much weaker than T_g , were characterized by their initial enthalpy at the solidus temperature. The liquid state enthalpy after quenching was $(-\Delta H_m \times \Delta\varepsilon_{lg0})$, or $(+\Delta H_m \times \Delta\varepsilon_{lg0})$, or 0 depending on its initial value before quenching and on the cooling and heating rates. The enthalpy increased from $-\Delta H_m \times \Delta\varepsilon_{lg0}$ and 0 up to $+\Delta H_m \times \Delta\varepsilon_{lg0}$ at T_m with configuron melting. The enthalpy decreased from $+\Delta H_m \times \Delta\varepsilon_{lg0}$ and 0 to $-\Delta H_m \times \Delta\varepsilon_{lg0}$ at T_m , rebuilding the missing bonds. These phenomena were well described by the positive or negative variation $\pm\Delta H_m \times \Delta\varepsilon_{lg}(T_{n+})$, of enthalpies of bonds and configurons.

Our homogeneous nucleation model above T_m still confirmed the formation of colloids between T_{n+} and T_m and at slow cooling rate, the growth of cluster-bound colloids inducing crystallization. The temperature T_{n+} , congruent materials being unique, was the temperature of homogenization of these melts. The highest temperature $T_{n+} = T_{LL}$ observed in $Pd_{42.5}Ni_{42.5}P_{15}$ and $La_{50}Al_{35}Ni_{15}$ was a homogenization temperature of these non-congruent materials. All melts, containing atoms of different nature, were submitted to short-range order inside superatoms, being the elementary bricks building the ordered liquids and glasses.

These colloids and elementary superatoms could not be more precisely described because their magic atom number n_c , and the associated enthalpy depending on n_c , were unknown.

Colloids formed by homogeneous nucleation were superatoms containing magic atom numbers which were not totally melted above T_m and were fully melted by homogenous nucleation instead of surface melting at the highest temperature T_{n+} . They contained a critical atom number n_c defined by their Gibbs free energy equal or smaller than that of the homogeneous melt. They gave rise to new molecular entities by bonding and antibonding, as shown by the opposite values of their contribution to the enthalpy at T_{n+} . Superstructures of elementary superatoms grew during cooling down to their percolation temperature.

The Mpemba effect and its inverse were easily predicted from this description of materials melting, leading to three stable liquid states above the melting temperature and transitions between them. The transition at T_{n+} may have been not only the temperature where the mean-range order disappeared, but also a first-order transition temperature between two liquid states.

Author Contributions: Conceptualization, R.F.T. and M.I.O.; methodology, R.F.T.; software, R.F.T.; validation, R.F.T. and M.I.O.; formal analysis, R.F.T.; investigation, R.F.T.; resources, R.F.T. and M.I.O.; data curation, R.F.T.; writing—original draft preparation, R.F.T.; writing—review and editing, R.F.T. and M.I.O.; visualization, R.F.T.; supervision, R.F.T. and M.I.O. All authors have read and agreed to the published version of the manuscript.

Funding: This research received no external funding.

Institutional Review Board Statement: Not applicable.

Informed Consent Statement: Not applicable.

Data Availability Statement: The data underlying this article will be shared on reasonable request from the corresponding author.

Acknowledgments: Thanks to L.N.C.M.I., Grenoble Alpes University, Imperial College London.

Conflicts of Interest: The authors declare no conflict of interest.

References

- De Rango, P.; Lees, M.; Lejay, P.; Sulpice, A.; Tournier, R.; Ingold, M.; Germi, P.; Pernet, M. Texturing of magnetic materials at high temperature by solidification in a magnetic field. *Nature* **1991**, *349*, 770–772. [[CrossRef](#)]
- Tournier, R.F.; Beaugnon, E. Texturing by cooling a metallic melt in a magnetic field. *Sci. Technol. Adv. Mater.* **2009**, *10*, 014501. [[CrossRef](#)]
- Porcar, L.; De Rango, P.; Bourgault, D.; Tournier, R.F. *Magnetic Texturing of High-Tc Superconductors*; Gabovitch, A., Ed.; BoD-Books on demand: Norderstedt, Germany, 2012; p. 171.
- Turnbull, D. Kinetics of solidification of supercooled liquid mercury. *J. Chem. Phys.* **1952**, *20*, 411. [[CrossRef](#)]
- Vinet, P.; Magnusson, L.; Frederiksen, H.; Desré, P.J. Correlations between surface and interface energies with respect to crystal nucleation. *J. Colloid Interf. Sci.* **2002**, *255*, 363–374. [[CrossRef](#)]
- Tournier, R.F. Presence of intrinsic growth nuclei in overheated and undercooled liquid elements. *Phys. B* **2007**, *392*, 79–91. [[CrossRef](#)]
- Tournier, R.F. Influence of Fermi energy equalization on crystal nucleation in glass melts. *J. Alloys Comp.* **2009**, *483*, 94–96. [[CrossRef](#)]
- Tournier, R.F. Thermodynamic origin of the vitreous transition. *Materials* **2011**, *4*, 869–892. [[CrossRef](#)]
- Tournier, R.F. Fragile-to-fragile liquid transition at T_g and stable-glass phase nucleation rate maximum at the Kauzmann temperature. *Phys. B* **2014**, *454*, 253–271. [[CrossRef](#)]
- Wool, R.P. Twinkling fractal theory of the glass transition. *J. Polym. Sci. Part B Polym. Phys.* **2008**, *46*, 2765–2778. [[CrossRef](#)]
- Wool, R.P.; Campanella, A. Twinkling fractal theory of the glass transition: Rate dependence and time-temperature superposition. *J. Polym. Sci. Part B Polym. Phys.* **2009**, *47*, 2578–2589. [[CrossRef](#)]
- Stanzione, J.F., III; Strawhecker, K.E.; Wool, R.P. Observing the twinkling nature of the glass transition. *J. Non-Cryst. Sol.* **2011**, *357*, 311. [[CrossRef](#)]
- Ojovan, M.I.; Travis, K.P.; Hand, R.J. Thermodynamic parameters of bonds in in glassy materials from viscosity temperature relationships. *J. Phys. Cond. Matter.* **2007**, *19*, 415107. [[CrossRef](#)] [[PubMed](#)]
- Ojovan, M.I.; Lee, W.E. Connectivity and glass transition in disordered oxide systems. *J. Non-Cryst. Sol.* **2010**, *356*, 2534–2540. [[CrossRef](#)]
- Ojovan, M.I. Ordering and structural changes at the glass-liquid transition. *J. Non-Cryst. Sol.* **2013**, *382*, 79. [[CrossRef](#)]
- Ojovan, M.I. Louzguine Luzgin, D.V. Revealing structural changes at glass transition via radial distribution functions. *J. Phys. Chem. B.* **2020**, *124*, 3186–3194. [[CrossRef](#)] [[PubMed](#)]

17. Sanditov, D.S.; Ojovan, M.I.; Darmaev, M.V. Glass transition criterion and plastic deformation of glass. *Phys. B* **2020**, *582*, 411914. [[CrossRef](#)]
18. Tournier, R.F.; Ojovan, M.I. Undercooled Phase Behind the Glass Phase with Superheated Medium-Range Order above Glass Transition Temperature. *Phys. B* **2021**, *602*, 412542. [[CrossRef](#)]
19. Tournier, R.F.; Ojovan, M.I. Dewetting temperatures of prefrozen and grafted layers in ultrathin films viewed as melt-memory effects. *Phys. B* **2021**, *611*, 412796. [[CrossRef](#)]
20. Xu, W.; Sandor, M.T.; Yu, Y.; Ke, H.-B.; Zhang, H.-B.; Li, M.-Z.; Wang, M.-Z.; Liu, L.; Wu, Y. Evidence of liquid-liquid transition in glass-forming $\text{La}_{50}\text{Al}_{35}\text{Ni}_{15}$ melt above liquidus temperature. *Nat. Commun.* **2015**, *6*, 7696. [[CrossRef](#)]
21. Chen, E.-Y.; Peng, S.-X.; Peng, L.; Michiel, M.D.; Vaughan, G.B.M.; Yu, Y.; Yu, H.-B.; Ruta, B.; Wei, S.; Liu, L. Glass-forming ability correlated with the liquid-liquid transition in $\text{Pd}_{42.5}\text{Ni}_{42.5}\text{P}_{15}$ alloy. *Scr. Mater.* **2021**, *193*, 117–121. [[CrossRef](#)]
22. Tanaka, H. Liquid-liquid transition and polyamorphism. *J. Chem. Phys.* **2020**, *153*, 130901. [[CrossRef](#)] [[PubMed](#)]
23. Popel, P.S.; Chikova, O.A.; Matveev, V.M. Metastable colloidal states of liquid metallic solutions. *High Temp. Mater. Proc.* **1995**, *4*, 219–233. [[CrossRef](#)]
24. Popel, P.S.; Sidorov, V.E. Microheterogeneity of liquid metallic solutions and its influence on the structure and properties of rapidly quenched alloys. *Mater. Sci. Eng.* **1997**, *A226–2289*, 237–244. [[CrossRef](#)]
25. Dahlborg, U.; Calvo-Dahlborg, M.; Popel, P.S.; Sidorov, V.R. Structure and properties of some glass-forming liquid alloys. *Eur. Phys. J.* **2000**, *B14*, 639–648. [[CrossRef](#)]
26. Manov, V.; Popel, P.; Brook-Levinson, F.; Molokanov, V.; Calvo-Dahlborg, M.; Dahlborg, U.; Sidorov, V.; Son, L.; Tarakanov, Y. Influence of the treatment of melt on the properties of amorphous materials: Ribbons, bulks and glass coated microwires. *Mater. Sci. Eng.* **2001**, *A304–A306*, 54–60. [[CrossRef](#)]
27. Popel, P.; Dahlborg, U.; Calvo-Dahlborg, M. On the existence of metastable microheterogeneities in metallic melts. *IOP Conf. Ser. Mater. Sci. Eng.* **2017**, *192*, 012012. [[CrossRef](#)]
28. Yang, B.; Perepezko, J.H.; Schmelzer, J.W.P.; GaO, Y.; Schick, C. Dependence of crystal nucleation on prior liquid overheating by differential fast scanning calorimeter. *J. Chem. Phys.* **2014**, *140*, 104513. [[CrossRef](#)]
29. He, Y.; Li, J.; Wang, J.; Kou, H.; Beaunon, E. Liquid-liquid structure transition and nucleation in undercooled Co-B eutectic alloys. *Appl. Phys. A* **2017**, *123*, 391. [[CrossRef](#)]
30. Adams, G.; Gibbs, J.H. On the temperature dependence of cooperative relaxation properties in glass-forming liquids. *J. Chem. Phys.* **1965**, *43*, 139. [[CrossRef](#)]
31. Liu, C.-Y.; He, J.; Keunings, R.; Bailly, C. New linearized relation for the universal viscosity-temperature behavior of polymer melts. *Macromolecules* **2006**, *39*, 8867–8869. [[CrossRef](#)]
32. Tournier, R.F. Thermodynamic and kinetic origin of the vitreous transition. *Intermetallics* **2012**, *30*, 104–110. [[CrossRef](#)]
33. Tournier, R.F. Predicting glass-to-glass and liquid-to-liquid phase transitions in supercooled water using classical nucleation theory. *Chem. Phys.* **2018**, *500*, 45–53. [[CrossRef](#)]
34. Tournier, R.F. Homogeneous nucleation of phase transformations in supercooled water. *Phys. B* **2020**, *579*, 411895. [[CrossRef](#)]
35. Tournier, R.F. First-order transitions in glasses and melts induced by solid superclusters nucleated by homogeneous nucleation instead of surface melting. *Chem. Phys.* **2019**, *524*, 40–54. [[CrossRef](#)]
36. Angell, C.A.; Rao, K.J. Configurational excitations in condensed matter and the “bond lattice”. Model for the liquid-glass transition. *J. Chem. Phys.* **1972**, *57*, 470–481. [[CrossRef](#)]
37. Iwashita, T.; Micholson, D.M.; Egami, T. Elementary excitations and crossover phenomenon in liquids. *Phys. Rev. Lett.* **2013**, *110*, 205504. [[CrossRef](#)] [[PubMed](#)]
38. Ozhovan, M.I. Topological characteristics of bonds in SiO_2 and GeO_2 oxide systems at glass-liquid transition. *J. Exp. Theor. Phys.* **2006**, *103*, 819–829. [[CrossRef](#)]
39. Benigni, P. Coupling of phase diagrams and thermochemistry. *Calphad* **2021**, *72*, 102228.
40. Wunderlich, B. Study of the change in specific heat of monomeric and polymeric glasses during the glass transition. *J. Chem. Phys.* **1960**, *64*, 1052. [[CrossRef](#)]
41. Kim, Y.H.; Kiraga, K.; Inoue, A.; Masumoto, T.; Jo, H.H. Crystallization and high mechanical strength of Al-based amorphous alloys. *Mater. Trans.* **1994**, *35*, 293–302. [[CrossRef](#)]
42. Hu, Q.; Sheng, H.C.; Fu, M.W.; Zeng, X.R. Influence of melt temperature on the Invar effect in $(\text{Fe}_{71.2}\text{B}_{0.24}\text{Y}_{4.8})_{96}\text{Nb}_4$ bulk metallic glasses. *J. Mater. Sci.* **2019**, *48*, 6900–6906.
43. Jiang, H.-R.; Bochtler, B.; Riegler, S.S.; Wei, X.-S.; Neuber, N.; Frey, M.; Gallino, I.; Busch, R.; Shen, J. Thermodynamic and kinetic studies of the Cu-Zr-Al(-Sn) bulk metallic glasses. *J. Alloys Comp.* **2020**, *844*, 156126. [[CrossRef](#)]
44. Yue, Y. Experimental evidence for the existence of an ordered structure in a silicate liquid above its liquidus temperature. *J. Non-Cryst. Sol.* **2004**, *345–346*, 523–527. [[CrossRef](#)]
45. Wei, S.; Yang, F.; Bednarcik, J.; Kaban, I.; Shuleshova, O.; Meyer, A.; Busch, R. Liquid-liquid transition in a strong bulk metallic glass-forming liquid. *Nat. Commun.* **2013**, *4*, 2083. [[CrossRef](#)] [[PubMed](#)]
46. Way, C.; Wadhwa, P.; Busch, R. The influence of shear rate and temperature on the viscosity and fragility of the $\text{Zr}_{41.2}\text{Ti}_{13.8}\text{Cu}_{12.5}\text{Ni}_{10.0}\text{Be}_{22.5}$ metallic-glass-forming liquid. *Acta Mater.* **2007**, *55*, 2977–2983. [[CrossRef](#)]
47. Lan, L.; Ren, Y.; Wei, X.Y.; Wang, B.; Gilbert, E.P.; Shibayama, T.; Watanabe, S.; Ohnuma, M.; Wang, X.-L. Hidden amorphous phase and reentrant supercooled liquid in Pd-Ni-P metallic glass. *Nat. Commun.* **2017**, *8*, 14679. [[CrossRef](#)]

48. Tournier, R.F. Glass phase and other multiple liquid-to-liquid transitions resulting from two-liquid competition. *Chem. Phys. Lett.* **2016**, *665*, 64–70. [[CrossRef](#)]
49. Wang, L.-M.; Borick, S.; Angell, C.A. An electrospray technique for hyperquenched glass calorimetry studies: Propylene glycol and di-n-butylphthalate. *J. Non-Cryst. Sol.* **2007**, *353*, 3829–3837. [[CrossRef](#)]
50. Hornboll, L.; Yue, Y. Enthalpy relaxation in hyperquenched glasses of different fragility. *J. Non-Cryst. Sol.* **2008**, *354*, 1832–1870. [[CrossRef](#)]
51. Hu, L.; Zhang, C.; Yue, Y. Thermodynamic anomaly of the sub- T_g relaxation in hyperquenched metallic glasses. *J. Chem. Phys.* **2013**, *138*, 174508. [[CrossRef](#)]
52. Passamani, F.C.; Tagarro, J.R.B.; Lareka, C.; Fernades, A.A.R. Thermal studies and magnetic properties of mechanical alloyed Fe₂B. *J. Phys. Cond. Mater.* **2002**, *14*, 1975–1983. [[CrossRef](#)]
53. Tournier, R.F. Crystallization of supercooled liquid elements induced by superclusters containing magic atom numbers. *Metals* **2014**, *4*, 359–387. [[CrossRef](#)]
54. Mpemba, E.B.; Osborne, D.G. Cool? *Phys. Educ.* **1969**, *4*, 172–175. [[CrossRef](#)]
55. Aristotle; Ross, W.D. *Aristotle's Metaphysics*; Clarendon: Oxford, UK, 1923.
56. Takaiwa, D.; Atano, I.; Koga, K.; Tanaka, H. Phase diagram of water in carbon nanotubes. *PNAS* **2008**, *105*, 39–43. [[CrossRef](#)] [[PubMed](#)]
57. Raju, M.; Van Duin, A. Phase transitions of ordered ice in graphene nanocapillaries and carbon nanotubes. *Sci. Rep.* **2018**, *8*, 3851. [[CrossRef](#)] [[PubMed](#)]
58. Nie, G.X.; Huang, J.Y.; Huang, J.P. Melting-freezing transition of monolayer water confined by phosphorene plates. *J. Phys. Chem. B* **2016**, *120*, 9011–9018. [[CrossRef](#)]
59. Lu, Z.; Raz, O. Nonequilibrium thermodynamics of the markovian Mpemba effect and its inverse. *PNAS* **2017**, *114*, 5883–5888. [[CrossRef](#)]
60. Kumar, A.; Bechhoefer, J. Exponentially faster cooling in a colloidal system. *Nature* **2020**, *584*, 64–68. [[CrossRef](#)]
61. Kuzmin, V.I.; Tytik, D.L.; Belashchenko, D.K.; Sirenko, A.V. Structure of silver cluster with magic numbers of atoms by data of molecular thermodynamics. *Colloid. J.* **2008**, *70*, 284–296. [[CrossRef](#)]
62. Wu, Q.; Xu, C.; Wu, X.; Cheng, L. Evidence for the super-atom bonding from bond energies. *ACS Omega*. **2018**, *3*, 14425–14430.
63. Koley, S.; Cui, J.Y.; Panfil, E.; Banin, U. Coupled colloidal quantum dot molecules. *Account Chem. Phys.* **2021**, in press. [[CrossRef](#)] [[PubMed](#)]